Impact of equatorial and continental airflow on primary greenhouse gases in the northern South China Sea

2015 Environ. Res. Lett. 10 065005

(http://iopscience.iop.org/1748-9326/10/6/065005)

Environmental Research Letters

OPEN ACCESS

RECEIVED
15 January 2015

REVISED
7 May 2015

ACCEPTED FOR PUBLICATION
7 May 2015

PUBLISHED
2 June 2015

LETTER

Impact of equatorial and continental airflow on primary greenhouse gases in the northern South China Sea

Chang-Feng Ou-Yang[1,2], Ming-Cheng Yen[1], Tang-Huang Lin[3], Jia-Lin Wang[2], Russell C Schnell[4], Patricia M Lang[4], Somporn Chantara[5] and Neng-Huei Lin[1,2,5]

[1] Department of Atmospheric Sciences, National Central University, Chung-Li, Taiwan
[2] Department of Chemistry, National Central University, Chung-Li, Taiwan
[3] Center for Space and Remote Sensing Research, National Central University, Chung-Li, Taiwan
[4] NOAA ESRL GMD, Boulder, USA
[5] Chemistry Department and Environmental Science Program, Chiang Mai University, Chiang Mai, Thailand

E-mail: nhlin@cc.ncu.edu.tw

Keywords: carbon dioxide (CO_2), methane (CH_4), Dongsha Island (DSI), South China Sea (SCS), Greenhouse Gases Observing Satellite (GOSAT), 7-SEAS

Supplementary material for this article is available online

Abstract

Four-year ground-level measurements of the two primary greenhouse gases (carbon dioxide (CO_2) and methane (CH_4)) were conducted at Dongsha Island (DSI), situated in the northern South China Sea (SCS), from March 2010 to February 2014. Their mean mixing ratios are calculated to be 396.3 ± 5.4 ppm and 1863.6 ± 50.5 ppb, with an annual growth rate of +2.19 ± 0.5 ppm yr^{-1} and +4.70 ± 4.4 ppb yr^{-1} for CO_2 and CH_4, respectively, over the study period. Our results suggest that the Asian continental outflow driven by the winter northeast monsoon could have brought air pollutants into the northern SCS, as denoted by significantly elevated levels of 6.5 ppm for CO_2 and 59.6 ppb for CH_4, which are greater than the marine boundary layer references at Cape Kumukahi (KUM) in the tropical northern Pacific in January. By contrast, the summertime CH_4 at DSI is shown to be lower than that at KUM by 19.7 ppb, whereas CO_2 is shown to have no differences (<0.42 ppm in July) during the same period. Positive biases of the Greenhouse Gases Observing Satellite (GOSAT) L4B data against the surface measurements are estimated to be 2.4 ± 3.4 ppm for CO_2 and 43.2 ± 36.8 ppb for CH_4. The satellite products retrieved from the GOSAT showed the effects of anthropogenic emissions and vegetative sinks on land on a vertical profiling basis. The prevailing southeasterly winds originating from as far south as the equator or Southern Hemisphere pass through the lower troposphere in the northern SCS, forming a tunnel of relatively clean air masses as indicated by the low CH_4 mixing ratios observed on the DSI in summer.

1. Introduction

Carbon dioxide (CO_2) and methane (CH_4) are the most abundant anthropogenic greenhouse gases (GHGs) in the atmosphere. They contribute approximately 93.6% of the well-mixed GHGs to global radiative forcing in 2011 (IPCC 2013). An increase in GHG concentrations can affect the Earth's radiation balance, and, thus, may cause changes in climate. It is generally recognized that the current increase in CO_2 levels is driven by fossil fuel combustion and carbon release from the biosphere through changes in land use, such as deforestation. Fossil fuel combustion accounts for about 92% of total global emissions of the atmospheric CO_2, excluding those from forest fires and the use of wood fuel (Olivier *et al* 2014). The impact of the changes in land use on CO_2 from 1850 to 2000 was evaluated to be 12 to 35 ppm (Brovkin *et al* 2004, Matthews *et al* 2004). CH_4 has an absolute global warming potential (AGWP) of 34 W m^{-2} yr kg^{-1}, normalized to CO_2 with the inclusion of climate-carbon cycle feedback over a 100-year period (IPCC 2013). Recent studies have indicated that global levels of CH_4 have risen because of addition in emissions that were likely provoked by meteorological causes, such as anomalously high temperatures in the Arctic and substantial precipitation in the tropics (Rigby *et al* 2008, Dlugokencky *et al* 2009, Nisbet *et al* 2014). Consequently, the radiative forcing and AGWP of CH_4 may decrease as its concentration increases because of its overlapping absorption spectra and changing atmospheric lifetimes (Reisinger *et al* 2011). Soil is a source and a sink of CH_4 in the balance of methanogenesis and methanotrophy because microbial processes depend on soil texture, latitude, climate, meteorology, and land use (Dutaur and Verchot 2007, Chen *et al* 2014). Changes in land use systems, such as the conversion of tropical forests to pasturelands and the initialization of fertilizer use, could reduce CH_4 uptake (Verchot *et al* 2000, Palm *et al* 2002, Veldkamp *et al* 2008), which is often seen in developing countries. This 'land effect' can affect the local air quality as well as that in remote downwind areas, reflecting the concentrations of air pollutants emitted through anthropogenic activity or deforestation.

The South China Sea (SCS) is the largest marginal sea in the world, covering an area from 99° E to 121° E and from the equator to 23° N. It is situated between the Tibetan Plateau and the western Pacific warm pool, featuring warm and wet weather with individual monthly total rainfall of approximately 300–500 mm throughout the region (Chang *et al* 2005). It is subject to physical disturbances during various periods of time in a range from short-term events (e.g. typhoons) to seasonal changes (e.g. alternating Asian monsoons) as well as inter-annual oscillations (e.g. El Niño and Southern Oscillation) (Fu *et al* 1983, Chao *et al* 1996, Zhang *et al* 1997, D'Asaro *et al* 2014). The prevailing winds in the SCS typically blow from the northeast in winter and from the southwest in summer (Liu *et al* 2001, Metzger 2003, Chang *et al* 2005). Various countries, including China, the Philippines, Vietnam, Malaysia and Indonesia, etc, surround the SCS, and it receives massive quantities of air pollutants from the surrounding land. Because of the increasing urbanization and industrialization in East Asia over the past several decades, increasing emissions of sulfur and nitrogen compounds have affected air quality over the North Pacific (Wild and Akimoto 2001, Akimoto 2003, Ohara *et al* 2007), particularly when their transport is driven by Asian continental outflow. Mounting evidences of the long-range transport of air pollutants from East Asia to as far as North America have been reported in the literature (Jaffe *et al* 2003, Liang *et al* 2004, Cooper *et al* 2010, Ambrose *et al* 2011). During winter, the cold surges driven by frontal passages can also transport polluted air masses into the SCS (Hsu *et al* 2007, Ou-Yang *et al* 2013, Ashfold *et al* 2015). Biomass burning activities are pronounced repeatedly in the Indochina region of peninsular Southeast Asia every year in spring (Liu *et al* 2003, Pochanart *et al* 2003, Ou-Yang *et al* 2012, Reid *et al* 2013, Lin *et al* 2014, Ou-Yang *et al* 2014, Wai and Tanner 2014). Substantial fire activities associated with agriculture begins in the maritime Southeast Asia in July and end at the onset of the winter monsoon during October to November (Moron *et al* 2009, Reid *et al* 2012, Reid *et al* 2013). Moreover, more than half of the world's annual tonnage carried by merchant fleets passes through the Straits of Malacca, Sunda, and Lombok, with the majority of them continuing on to the SCS, making the SCS one of the most crucial trade routes in the world (US EIA 2013). In addition, the SCS has been suggested to be a moderate source of CO_2 emitted to the atmosphere through sea–air exchanges (Zhai *et al* 2005, Dai *et al* 2013). These events, regardless of whether they are caused by anthropogenic or natural activities, may contribute additional constituents to the atmosphere in this region.

To improve the scientific understanding of the role of Asian continental outflow and its effects on air quality, numerous intensive field campaigns have been conducted over the western Pacific (e.g. PEM-West B (Hoell *et al* 1997), BIBLE (Kondo *et al* 2002), TRACE-P (Jacob *et al* 2003), and EAREX (Nakajima *et al* 2007). More recently, the Seven Southeast Asian Studies (7-SEAS) program was launched to investigate the effect of biomass burning in the Indochina region on aerosol-environmental systems, cloud chemistry, atmospheric radiation, and regional climates (Lin *et al* 2013, Reid *et al* 2013, Tsay *et al* 2013). Based on respective approaches, these studies have demonstrated that the anthropogenic emissions from Southeast Asia could influence the composition of the Pacific troposphere. However, few studies on the atmospheric constituents of GHGs have focused on the SCS.

Here, we present 4-year observational data on primary GHGs observed at DSI from the perspectives of their seasonality and average levels representative of the northern SCS. Seasonal cycles of CO_2 and CH_4 at DSI are carefully assessed in comparison with the marine boundary layer (MBL) reference in the subtropical north Pacific. To evaluate the effects of respective inflows on the GHGs in this region, we also investigate the characteristics of the two GHGs associated with their source regions through the cluster analysis of backward trajectories. The retrieval products of satellite observations are used in this research to characterize the vertical and horizontal structure of the atmospheric GHGs in the SCS as well as to evaluate the land effects resulted from different influences. In addition, the biases of the satellite data against the surface measurements are estimated.

2. Methodology and data

2.1. Site description

Dongsha Island (DSI) (20.70° N, 116.73° E, 8 m a.s.l.) is a tiny atoll in the northern SCS, with an area of

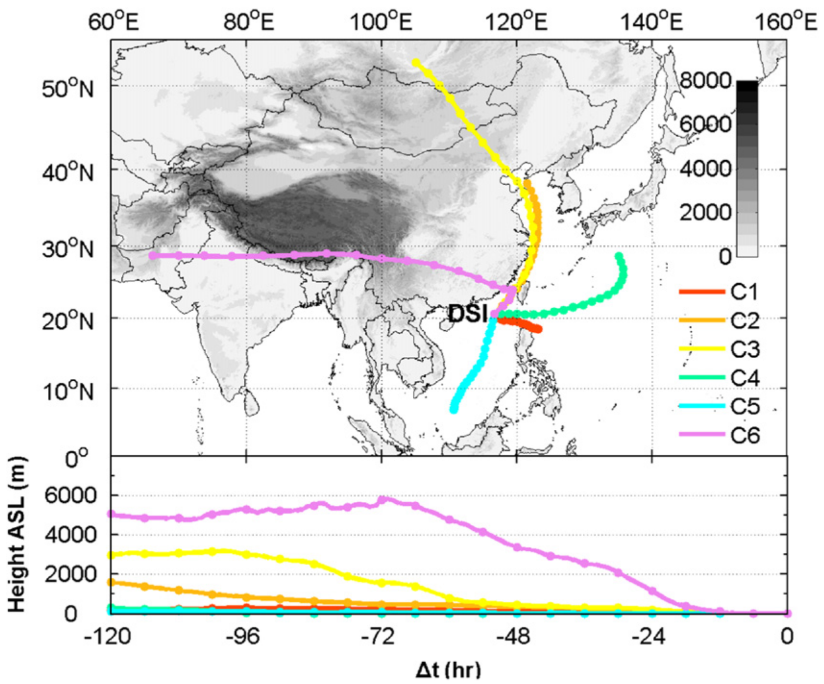

Figure 1. Geographic location and terrain map of the Dongsha Island (DSI) associated with classified mean backward trajectories.

1.74 km^2 and located approximately 440 km southwest of the southern tip of Taiwan. The nearest land is Shantou City, China, which is approximately 250 km to the north. Figure 1 illustrates the geographical location of DSI and the averaged backward trajectories based on cluster analysis (see further discussion in section 3.2). DSI is located on the pathway of the alternating Asian monsoons, and features a subtropical maritime climate. It serves as a remote downwind site of encountering frontal passages driven by the winter monsoon that originates from East Asia. While, in summer, DSI serves as a downwind site of monitoring the long-range transport of air masses originating from Indonesia or nearby areas. Detailed information on DSI can be also found in previous studies (Lin *et al* 2013, Ou-Yang *et al* 2013).

2.2. Flask air sampling

As a part of the Carbon Cycle Greenhouse Gases Network (CCGG), a pair of 2.5 L flask air samples was collected once per week in the morning at DSI by using a portable sampling unit and then shipped to National Oceanic and Atmospheric Administration/Earth System Research Laboratory/Global Monitoring Division (NOAA/ESRL/GMD) for analysis. The CO_2 and CH_4 were measured using nondispersive infrared spectroscopy and gas chromatography/flame ionization detection, respectively. Typical precisions of the analytical methods for CO_2 and CH_4 are <0.1 ppm and <1.5 ppb, respectively (Thoning *et al* 1995, Dlugokencky *et al* 2005). Detailed information about the analytical techniques for each GHG has been documented (Dlugokencky *et al* 1994, Thoning *et al* 1995). Standard scales used are the WMO X2007 CO_2 and NOAA04 CH_4 mole fractions. Any flask sample pair with a difference of 0.5 ppm or more in the CO_2 mixing ratio was flagged and not used in this study. To gain a wider view of the effects of Asian continental outflow on the GHGs in this region, Cape Kumukahi (KUM) (19.52° N, 154.82° E, 3 m a.s.l.), one of the CCGG sites and located in the mid-Pacific at a similar latitude to DSI, is used to represent the reference baseline GHG levels in the MBL in the Pacific. The analytical methods and data treatment are similar at DSI and KUM[6].

2.3. Trajectory analysis

Five-day (120 h) backward trajectories were calculated using the NOAA Air Resources Laboratory HYbrid Single-Particle Lagrangian Integrated Trajectory (HYSPLIT, Version 4.9) model (Draxler and Rolph 2014). The meteorological grid data used are the Global Data Assimilation System archives provided by the National Center for Environmental Prediction, with a 3-hourly and 1° × 1° latitude–longitude resolution. Trajectory deviation to approximately 20% of the traveled distance on average was suggested (Stohl 1998). In this study, all backward trajectories of every flask air sample collected at DSI are computed with an initial sampling inlet height of 8 m a.s.l. We also use cluster analysis to classify these

[6] Detailed descriptions of the sampling and measurement methods used are provided on the NOAA/ESRL/GMD website at www.esrl.noaa.gov/gmd/outreach/behind_the_scenes/measurementlab.html. The discrete flask air sampling data can also be found on their website at www.esrl.noaa.gov/gmd/dv/data/.

backward trajectories associated with the GHG measurements to assess their respective contributions at DSI.

2.4. Greenhouse gases observing satellite data

Ground-based measurements and satellite retrievals can be highly effective in investigating the seasonal and spatial characteristics of air pollutants and can provide new insights into the location and magnitude of sources and sinks on a regional scale. However, the accuracy of retrieved data must be assessed using direct measurements, particularly for sites located in the continental interior. Substantial effort has been expended to validate the column-averaged GHG retrievals against ground-based measurements from the Total Carbon Column Observing Network (Morino *et al* 2011, Parker *et al* 2011, Wunch *et al* 2011, Cogan *et al* 2012) or from aircraft measurements (Inoue *et al* 2014). Although the retrieval algorithm and the data processing methods were carefully refined and markedly improved (Yoshida *et al* 2013), their errors may be noticeable at locations near source or sink areas where land effects are pronounced.

The Greenhouse Gases Observing Satellite (GOSAT) was launched from Tanegashima Island in Japan on 23 January 2009 (Kuze *et al* 2009, Yokota *et al* 2009). It has an approximately 3-day repeat cycle and flies in a sun-synchronous orbit with an altitude of 665.96 km and inclination of 98.06°. The GOSAT is equipped with a thermal and near infrared sensor, a Fourier transform spectrometer, and cloud and aerosol imager operating on seven channels, three of which are in the short wavelength infrared region (0.76, 1.6 and 2 μm) and one of which is in thermal infrared spectra (5.5–14.3 μm) (Kuze *et al* 2009). The Level 4B products used in this study are derived from the GOSAT satellite retrievals by using a global 3-D atmospheric transport model with Level 4A global fluxes, offering global 3-D distributions of CO_2 (Version 2.02) and CH_4 (Version 1.01) with a 6-hourly time step and 2.5° × 2.5° horizontal resolution.[7] Nine layers of the GOSAT L4B data at geopotential heights ranging from the surface to approximately 6.5 km a.s.l. (i.e. 975, 925, 900, 850, 700, 600, 500, 400, and 300 hPa) from March 2010 to October 2011 for CO_2 and from March 2010 to May 2011 for CH_4 are used in this study.

3. Results and discussion

3.1. Seasonality of CO_2 and CH_4 at Dongsha Island

Figure 2 illustrates the time-dependent variations of CO_2 and CH_4 measured at DSI and KUM from March 2010 to February 2014. The mean mixing ratios of CO_2 and CH_4 at DSI are estimated to be 396.3 ± 5.4 ppm and 1863.6 ± 50.5 ppb, respectively, over the study period. Note that these uncertainties are calculated based on the standard deviation (1σ) of detrended data obtained by subtracting the increasing trends. Greater amplitudes within the CO_2 and CH_4 seasonal cycles can be found at DSI than those at KUM. The mean rates of annual growth of CO_2 and CH_4 at DSI are calculated to be +2.19 ± 0.5 ppm yr^{-1} and +4.70 ± 4.4 ppb yr^{-1}, respectively, during 2011 to 2014. The annual growth rate is determined by the average of November-February months in a given year subtracting the same four-month average centered on the previous January 1. The uncertainties of the CO_2 and CH_4 annual growth rates are calculated based on the standard errors (2σ) in slope of an average linear rate of increase fit to the CO_2 and CH_4 data at DSI over the study period as a crude estimate of the uncertainty. Note that the uncertainty should only be considered a lower bound to the actual uncertainty because it does not include a component of uncertainty for undersampling by collecting samples only once per week. The smoothed data illustrated as the lines in figure 2 is calculated by filtering out the residuals with a short-term cutoff of 80 days. The algorithm is adopted by the NOAA/ESRL/GMD (Thoning *et al* 1989). During the last decade, the baseline CO_2 mixing ratios have also increased in the surrounding countries of SCS, for instance, at a rate of 1.8 ppm yr^{-1} at Bukit Kototabang (0.20° S, 100.32° E, 864 m a.s.l.) in Indonesia from 2004 to 2011 (Nahas 2012) and at a rate of 1.9 ppm yr^{-1} at Danum Valley (4.95° N, 117.85° E, 426 m a.s.l.) in Malaysia from 2004 to 2013 (Jahaya *et al* 2013). As summarized by IPCC (2013), the global increases in CO_2 and CH_4 levels are reported to be 11.7 ppm and 29 ppb, respectively, during 2005 to 2011. Despite the possible differences or gradients in concentrations occurring within the lower troposphere, the GOSAT L4B data at 975 hPa (approximately 300 m a.s.l.) show seasonal patterns in the two GHGs similar to those at DSI with mean positive biases of 2.4 ± 3.4 ppm for CO_2 and 43.2 ± 36.8 ppb for CH_4; by contrast, relative to the surface measurements at KUM, the satellite data show smaller biases, exhibiting mean differences of less than 0.1 ± 1.0 ppm and 3.6 ± 10.5 ppb for CO_2 and CH_4, respectively. Nevertheless, a larger degree of the data divergence around the regression line can be seen in the elevated range of CO_2 and CH_4 at DSI (see supplementary materials), which is likely due to relatively inhomogeneous atmospheric composition while encountering polluted air masses from temporal and spatial perspectives. A significant deviating relationship in CH_4 is evident for the regression line of NOAA/ESRL/GMD flasks versus the GOSAT L4B products (see supplementary materials available at stacks.iop.org/ERL/10/065005/mmedia).

Distinct seasonal features with wintertime maxima and summertime minima are found for surface

[7] These satellite data can be requested on the official GOSAT website at https://data.gosat.nies.go.jp/gateway/gateway/MenuPage/open.do. Details on the data products and retrieval methods are also provided on their website at www.gosat.nies.go.jp/eng/gosat/info.htm and in the literature (Kuze *et al* 2009, Yoshida *et al* 2013).

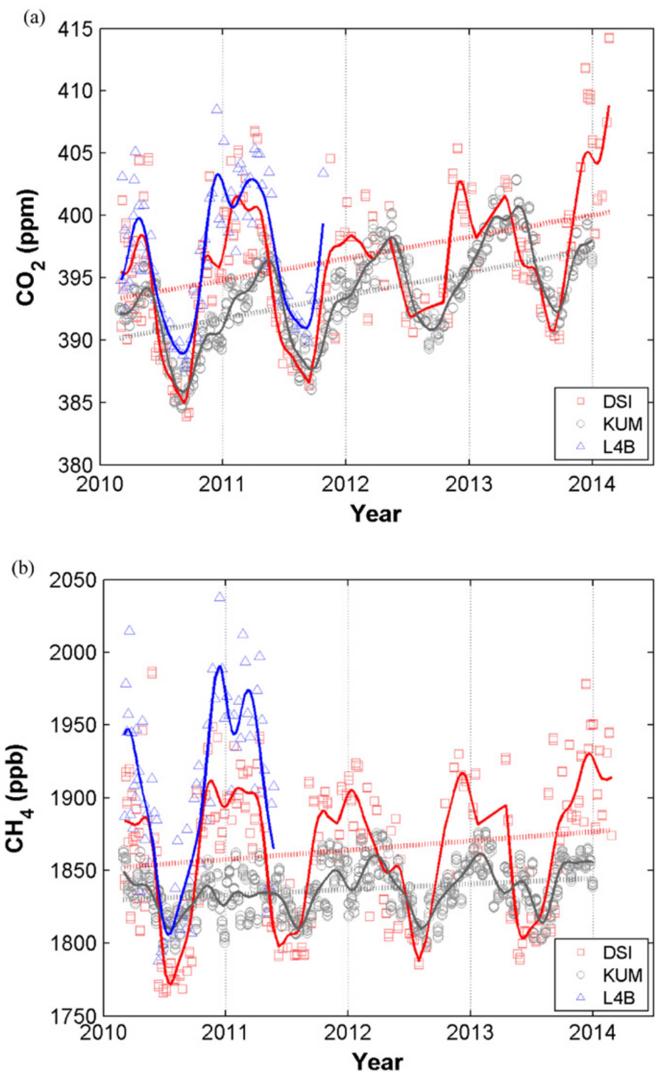

Figure 2. Time-series of (a) CO_2 and (b) CH_4 mixing ratios in the NOAA/GMD flask air samples at Dongsha Island (DSI, red open squares) from March, 2010 to February, 2014, and at Kumukahi (KUM, gray open circles) from March, 2010 to December, 2013. The blue open triangles represent the GOSAT L4B data at DSI. The solid lines are the smoothed fittings estimated based on the NOAA/GMD short-term filtering algorithm. The red and gray dotted lines display the increasing trends at DSI and KUM, respectively. Note that the data at DSI in 2014 are preliminary.

observational data and satellite retrievals, which showed similar patterns at other remote sites in the Northern Hemisphere (Conway *et al* 1994, Dlugokencky *et al* 1994). Mean levels of CO_2 and CH_4 at DSI and KUM during specific seasons are listed in table 1. In winter, the Asian continental high-pressure system dominates the transport of the outflow plume, leading to a direct effect on the levels of GHGs as well as the air quality in the neighboring downwind areas (Ou-Yang *et al* 2013). Due to the influences by maritime southwest monsoon flows in summer, DSI experiences low and steady background levels of GHGs in the northern SCS. Here, we adopt the GHG measurements obtained at KUM as the MBL reference at approximately 20° N in the Pacific. Comparing the ground-level observational results at KUM shows that the excessive amounts of GHGs from the combustion of fossil fuels and burning of biomass permeate the northern SCS Basin in winter and spring when the air is leaving the Asian continent, indicating significant increases in the winter maxima of CO_2 and CH_4 at DSI (figure 2). In January, the differences in the GHG concentrations between DSI and KUM are estimated to be 6.5 ppm for CO_2 and 59.6 ppb for CH_4. The cold fronts caused by the Siberian high pressure system in winter move southeastward, thus driving the Asian pollution outflow into the SCS (Zhang *et al* 1997, Liu *et al* 2003, Wang *et al* 2003). In summer, vegetation growth on land largely eliminates the CO_2 signal at DSI, which is as clear and stable as that measured at KUM. The CH_4 levels at DSI during the midsummer southwest monsoon period are lower than those at KUM by 19.7 ppb (figure 2(b)), whereas CO_2 is shown to have no differences (<0.42 ppm in July) during the same period. In addition, the amplitude of the annual cycle of monthly averaged CH_4 at DSI is estimated to be 108.3 ppb,

Table 1. Statistics of seasonal CO_2 and CH_4 mixing ratios observed at DSI and KUM.

	Number of pairs		CO_2 (ppm)				CH_4 (ppb)			
			DSI		KUM		DSI		KUM	
Season	DSI	KUM	Mean	Detrended Δ[a]	Mean	Detrended Δ[a]	Mean	Detrended Δ[a]	Mean	Detrended Δ[a]
Spring (MAM)	49	160	397.8	3.2 ± 4.2	396.2	0.1 ± 2.4	1864.7	2.2 ± 45.7	1842.5	−0.4 ± 17.1
Summer (JJA)	42	155	391.4	−4.2 ± 2.4	392.3	−0.2 ± 3.4	1806.4	−57.9 ± 28.3	1820.6	7.5 ± 14.3
Autumn (SON)	40	153	394.3	−1.7 ± 5.4	391.3	0.1 ± 3.6	1879.7	13.7 ± 41.4	1840.2	2.4 ± 12.4
Winter (DJF)	40	129	401.6	4.8 ± 3.8	394.7	−0.4 ± 3.1	1905.8	38.8 ± 24.4	1846.7	−1.4 ± 15.0
Overall	171	597	396.3	± 5.4[b]	393.6	± 3.1[b]	1863.6	± 50.5[b]	1837.1	± 16.9[b]

[a] The uncertainties are calculated based on 1σ.

[b] Only the uncertainties for the whole study period are calculated.

which is approximately three times greater than that of KUM at 36.1 ppb, indicating that surrounding lands exert a significant effect.

3.2. Source region characterization

Cluster analysis of backward trajectories is a common method for evaluating the contribution of air pollutants from respective source regions with respect to measurements at receptor sites. For the study period, 171 trajectories are computed and grouped into six clusters (figure 1). Each average trajectory represents a distinct route: C1 (western Pacific), C2 (east China), C3 (north China), C4 (local), C5 (SCS), and C6 (subsidence) (see supplementary materials for all trajectories in each cluster). The statistical frequencies for each cluster according to month are estimated as illustrated in figure 3, showing a clear seasonality of changes in air masses arriving at DSI. Our cluster analysis of the backward trajectories is similar to that of previous studies conducted at Hok Tsui, Hong Kong (Wang *et al* 2009, Ding *et al* 2013). However, no trajectory analyzed in this study passes directly through southern China. Air masses originating from China (C2 and C3) dominate during fall to late spring, accounting for 52.0% of the total trajectories. These air masses travel along the western Pacific coastline, a heavily polluted area in East Asia, showing relatively high levels of CO_2 and CH_4. The results concur with previous studies which have indicated that episodes of enhanced CO_2 or other air pollutants over the SCS are driven by the Asian outflow traveling with the winter monsoon (Vay *et al* 2003, Ou-Yang *et al* 2013). C2 and C3 are distinguished by their heights and distances, representing various transport speeds and residue times of air masses. However, no significant differences in the levels of GHGs are found between them (table 2). C4 represents aged air masses that are transported from the Asian continent and mixed with those from the Pacific, showing medium levels of GHGs (table 2). The C6 air masses contribute only approximately 3.5% of all trajectories. They are conveyed along with the westerly winds in the free troposphere and are rapidly dragged down to the surface by the downward branch of the transient local East-West cell/circulation, which was induced by the subsidence of a cold surge anticyclone (Yen *et al* 2013). These quick-moving air parcels merge with the southwesterly winds at the end of their transport approximately 1 day before arriving at DSI, exhibiting the highest level of GHGs among all groups (table 2). The C1 group consists of the local air in the northern SCS and is primarily present during the transition period between spring and summer when the pathway of air masses rotates clockwise. In summer, the marine air primarily originates from the SCS (C5), accounting for 56.3% of all trajectories in July. Several cross-equatorial airflows are present from Indonesia to the SCS (see supplementary materials). The C5 air masses exhibit the lowest levels of ΔCO_2 (−2.3 ± 3.0 ppm) and ΔCH_4 (−20.9 ± 30.2 ppb).

3.3. Vertical profiles of greenhouse gases in the South China Sea

Figure 4 shows a selected longitude–latitude slice of monthly average CO_2 and CH_4 mixing ratios in the GOSAT L4B data at latitude of 20° N in the Pacific atmosphere in winter (January 2011) and summer (July 2010). Elevated CO_2 levels are found in the surface layer (below 850 hPa) between 100° E and 120° E (figure 4(a), top panel), indicating that a concise air flow penetrates this region from the east edge of East Asia. The highly polluted continental air masses traveling with the winter monsoon spread as far as 150° E at a latitude of 20° N, as shown in the CO_2 and CH_4 cross sections. However, in contrast to CO_2, a relatively high level of CH_4 is observed on the east coast of the Bay of Bengal and in Myanmar at this latitude in winter (figure 4(a), bottom panel) and summer (figure 4(b), bottom panel). Stable and steady characteristics are observed for the two GHGs in the eastern part of the Pacific atmosphere (120° W–150° W) at the same time. No significant differences in CO_2 are evident in the summer between DSI and KUM (figure 2(a)). The inconsistency in the levels of CO_2 in the slice over the entire Pacific is less than 3 ppm, which is close to the bias of column-averaged

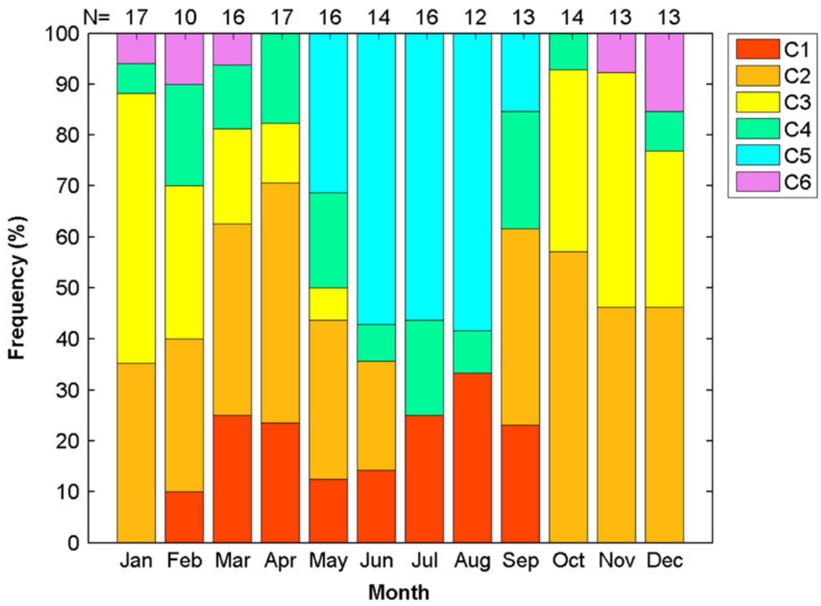

Figure 3. Frequencies of classified trajectories in each month. The number of trajectories calculated is listed on the top.

dry-air mixing ratios (1.48 ± 2.09 ppm) reported by Yoshida *et al* (2013). However, the land effect might partially remove atmospheric CO_2 in the Indochina region in summer (figure 4(b), top panel). The CH_4 vertical profiles show a 'window' of relatively low concentrations below 700 hPa (figure 4(b), bottom panel), implying that there is a tunnel in the northern SCS for the clean air masses from the lower latitudes or Southern Hemisphere to pass through. This phenomenon could be resulted from the migration of intertropical convergence zone occurred during summer (Lawrence 2004). A steep gradient in CH_4 mixing ratios from land to sea is observed near the surface at approximately 105° E in summer, forming a wall cut by the southwesterly inflows. This window characteristic is not clear for CO_2 because of the relatively higher CO_2 level in the air masses from the lower latitudes in summer. In addition, low spatial variability of GHGs above 700 hPa can be seen over the SCS, indicating minimal seasonal variations and unclear influences from land (see supplementary material available at available at stacks.iop.org/ERL/10/065005/mmedia).

Figure 5 shows a time series of daily average vertical profiles of CO_2 and CH_4 mixing ratios at DSI extracted from the GOSAT L4B data from March 2010 to February 2011. Although the discrepancies between the L4B products and the surface measurements are negligible (<0.6% for CO_2 and <2.3% for CH_4), the GOSAT satellite has a 3-day repeat global cycle (Yokota *et al* 2009), which may induce several minor errors in the results within 1–2 days. As illustrated in figure 5, enhanced GHG levels are found within the lower troposphere (below approximately 700 hPa geopotential height) from early winter to late spring, particularly for the layers near the surface (below approximately 900 hPa), which is consistent with the results of the aforementioned cluster analysis of backward trajectories in association with surface measurements. During summer, no substantial concentration gradients in CO_2 are found in the air column within the entire troposphere. The 'window' opens to sweep the primary air pollutants, such as CH_4, in the northern SCS from July to August, showing that the summertime CH_4 mixing ratio measured at DSI is lower compared with that at KUM in the mid-Pacific.

4. Conclusion

In this paper, we first present the 4-year ground-level measurements of primary GHGs (i.e. CO_2 and CH_4) at DSI as a representative site for monitoring background air quality in the northern SCS. Increased mixing ratios for the two compounds are observed at DSI and are identified to be caused by the Asian continental outflow. The enhanced levels are calculated to be 6.5 ppm and 59.6 ppb for CO_2 and CH_4, respectively, in January. No significant difference (<0.42 ppm in July) in summertime CO_2 levels between DSI and KUM (which represents the MBL reference at approximately 20° N in the Pacific) is evident. However, the summertime CH_4 levels at DSI are relatively low and differ from those at KUM by 19.7 ppb in July, likely because of the inflows of maritime air masses originating at low latitudes of the SCS. By integrating the satellite retrieval products of the GOSAT, the land effects caused by respective sources are shown in association with backward trajectory clustering. The deviations of GOSAT L4B data from the surface measurements are assessed, and positive biases of

Table 2. Statistics of CO_2 and CH_4 mixing ratios for different trajectory clusters at DSI.

Cluster	Number	%	CO_2 (ppm)	CH_4 (ppb)	ΔCO_2 (ppm)[a]	ΔCH_4 (ppb)[a]
1 (local)	24	14.0	392.9 ± 3.9	1820.7 ± 32.7	−0.9 ± 3.3	−10.4 ± 27.4
2 (east China)	56	32.7	398.8 ± 5.2	1895.9 ± 34.4	4.6 ± 4.6	54.9 ± 33.1
3 (north China)	33	19.3	399.3 ± 5.0	1904.4 ± 24.0	5.4 ± 4.5	60.8 ± 23.4
4 (western Pacific)	21	12.3	393.3 ± 4.1	1836.1 ± 28.9	0.0 ± 3.2	0.9 ± 21.8
5 (South China Sea)	31	18.1	390.5 ± 3.5	1804.1 ± 29.2	−2.6 ± 2.8	−20.1 ± 30.6
6 (subsidence)	6	3.5	402.6 ± 6.4	1909.2 ± 23.5	8.2 ± 5.9	64.3 ± 22.2

[a] The differences are calculated by the CO_2 and CH_4 levels of the individual trajectory subtracting the correlated monthly mean of the smoothed data at KUM.

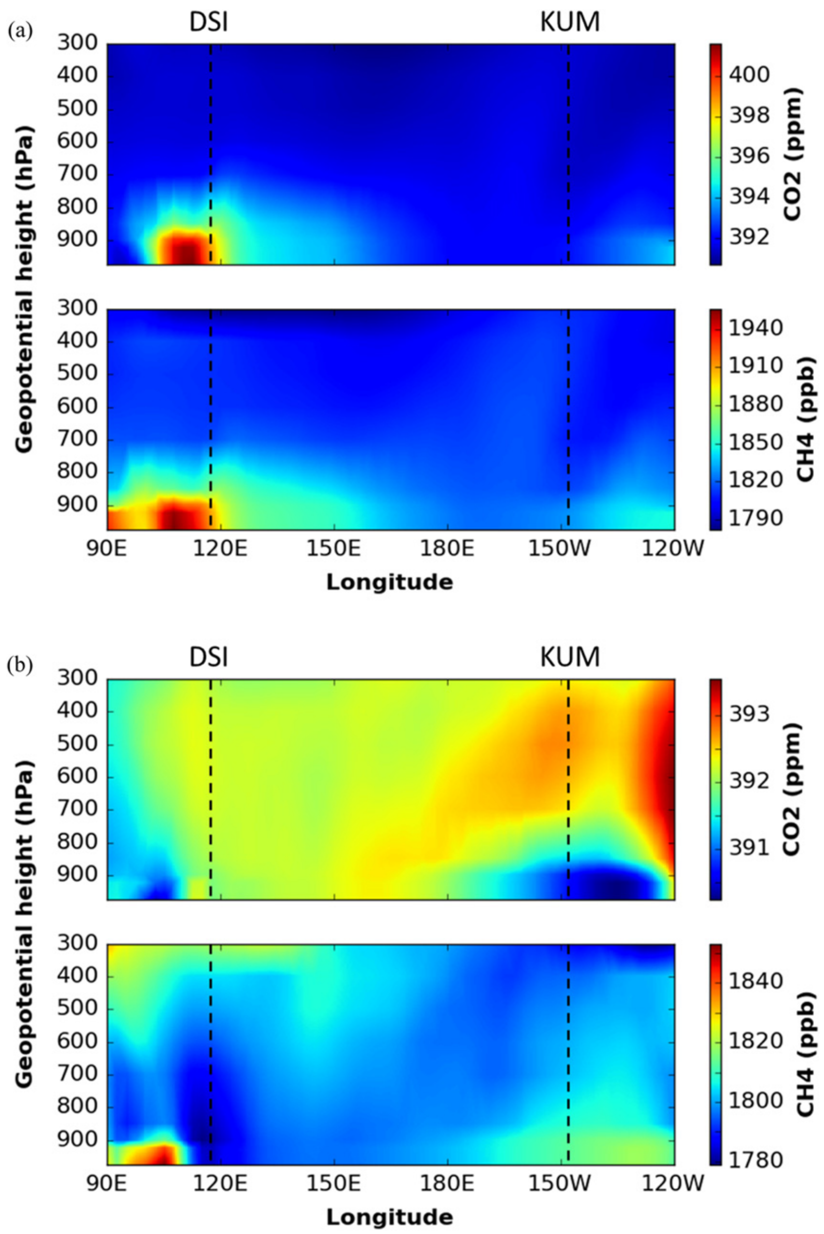

Figure 4. Longitude–altitude cross-section of CO_2 and CH_4 vertical profiles at latitude of 20°N over the Pacific region in (a) January 2011 and (b) July 2010. Note that the concentration scales are deliberately set differently for better illustrating the gradients of CO_2 and CH_4 levels in respective seasons.

2.4 ± 3.4 ppm for CO_2 and 43.2 ± 36.8 ppb for CH_4 are found at DSI, showing greater discrepancies in the continental interior than those at KUM in the mid-Pacific. The results provided in this study may strengthen the understanding of how this relatively unpolluted region receives Asian continental outflow from higher latitudes and purged with maritime inflows from lower latitudes in respective seasons.

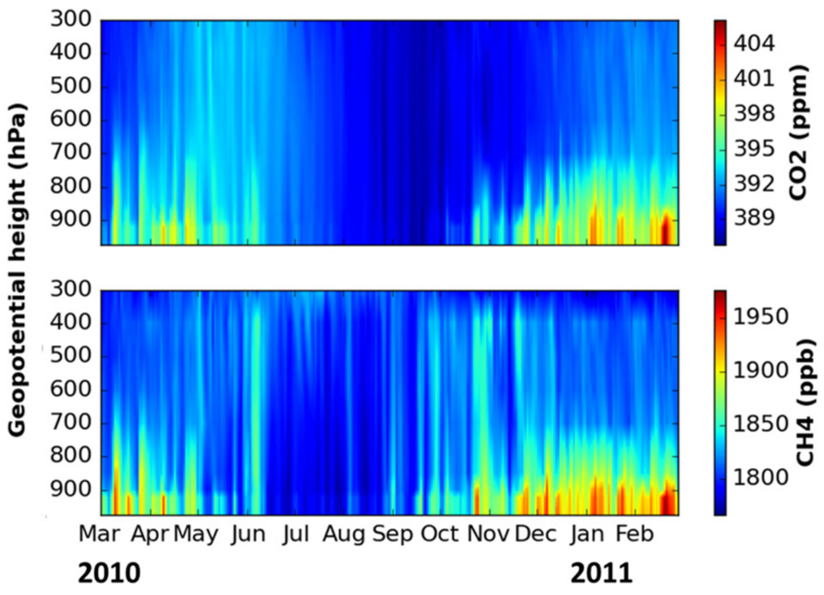

Figure 5. A year of daily-averaged vertical profiles of CO_2 and CH_4 mixing ratios at DSI.

Acknowledgments

We are grateful to Japan Aerospace Exploration Agency, National Institute for Environmental Studies, and Japan Ministry of the Environment for releasing the GOSAT data used in our study. This work was financially supported by the Taiwan Environmental Protection Agency under contracts EPA-99-U1L1-02-101, EPA-100-U1L1-02-101, EPA-101-U1L1-02-101, and EPA-102-U1L1-02-101 and by the Taiwan Ministry of Sciences and Technology, formerly Taiwan National Science Council, under contracts NSC 99-2111-M-008-011, NSC 100-2111-M-008-011, NSC 101-2119-M-008-012, NSC 102-2111-M-008-005, and MOST 103-2111-M-008-001. The authors thank the NOAA/ARL for providing the HYSPLIT trajectory model and/or READY website (http://ready.arl.noaa.gov) that were used in this study. We also thank Dr Jin-Yi Yu at University of California, Irvine, for his valuable comments on the transport patterns of equatorial air masses.

References

Akimoto H 2003 Global air quality and pollution *Science* **302** 1716–9

Ambrose J L, Reidmiller D R and Jaffe D A 2011 Causes of high O_3 in the lower free troposphere over the pacific northwest as observed at the Mt. Bachelor observatory *Atmos. Environ.* **45** 5302–15

Ashfold M J *et al* 2015 Rapid transport of East Asian pollution to the deep tropics *Atmos. Chem. Phys.* **15** 3565–73

Brovkin V, Sitch S, von Bloh W, Claussen M, Bauer E and Cramer W 2004 Role of land cover changes for atmospheric CO_2 increase and climate change during the last 150 years *Global Change Biol.* **10** 1253–66

Chang C P, Wang Z, McBride J and Liu C H 2005 Annual cycle of Southeast Asia—maritime continent rainfall and the asymmetric monsoon transition *J. Climate* **18** 287–301

Chao S Y, Shaw P T and Wu S Y 1996 El Nino modulation of the South China Sea circulation *Prog. Oceanogr.* **38** 51–93

Chen Y J, Day S D, Shrestha R K, Strahm B D and Wiseman P E 2014 Influence of urban land development and soil rehabilitation on soil-atmosphere greenhouse gas fluxes *Geoderma.* **226** 348–53

Cogan A J *et al* 2012 Atmospheric carbon dioxide retrieved from the Greenhouse gases Observing SATellite (GOSAT): Comparison with ground-based TCCON observations and GEOS-Chem model calculations *J. Geophys. Res.* **117** D21301

Conway T J, Tans P P, Waterman L S and Thoning K W 1994 Evidence for interannual variability of the carbon cycle from the national oceanic and atmospheric administration/climate monitoring and diagnostics laboratory global air sampling network *J. Geophys. Res.* **99** 22831–55

Cooper O R *et al* 2010 Increasing springtime ozone mixing ratios in the free troposphere over western North America *Nature* **463** 344–8

D'Asaro E A *et al* 2014 Impact of Typhoons on the Ocean in the pacific *B. Am. Meteorol. Soc.* **95** 1405–18

Dai M H, Cao Z M, Guo X H, Zhai W D, Liu Z Y, Yin Z Q, Xu Y P, Gan J P, Hu J Y and Du C J 2013 Why are some marginal seas sources of atmospheric CO_2? *Geophys. Res. Lett.* **40** 2154–8

Ding A J, Wang T and Fu C B 2013 Transport characteristics and origins of carbon monoxide and ozone in Hong Kong, South China *J. Geophys. Res.* **118** 9475–88

Dlugokencky E J, Steele L P, Lang P M and Masarie K A 1994 The growth rate and distribution of atmospheric methane *J. Geophys. Res.* **99** 17021–43

Dlugokencky E J, Myers R C, Lang P M, Masarie K A, Crotwell A M, Thoning K W, Hall B D, Elkins J W and Steele L P 2005 Conversion of NOAA atmospheric dry air CH_4 mole fractions to a gravimetrically prepared standard scale *J. Geophys. Res.* **110**

Dlugokencky E J *et al* 2009 Observational constraints on recent increases in the atmospheric CH_4 burden *Geophys. Res. Lett.* **36** L18803

Draxler R R and Rolph G D 2014 HYSPLIT (HYbrid Single-Particle Lagrangian Integrated Trajectory) Model access via NOAA ARL READY (http://ready.arl.noaa.gov/HYSPLIT.php)

Dutaur L and Verchot L V 2007 A global inventory of the soil CH_4 sink *Global. Biogeochem. Cy.* **21** GB 4013

Fu C, Fletcher J and Slutz R 1983 The Structure of the asian monsoon surface wind field over the ocean *J. Clim. Appl. Meteorol.* **22** 1242–52

Hoell J M, Davis D D, Liu S C, Newell R E, Akimoto H, McNeal R J and Bendura R J 1997 The pacific exploratory mission-west phase B: february-march, 1994 *J. Geophys. Res.* **102** 28223–39

Hsu S C, Liu S C, Kao S J, Jeng W L, Huang Y T, Tseng C M, Tsai F, Tu J Y and Yang Y 2007 Water-soluble species in the marine aerosol from the northern South China Sea: High chloride depletion related to air pollution *J. Geophys. Res.* **112** D19304

Inoue M *et al* 2014 Validation of XCH4 derived from SWIR spectra of GOSAT TANSO-FTS with aircraft measurement data *Atmos. Meas. Tech.* **7** 2987–3005

IPCC 2013 *Climate Change 2013: The Physical Science Basis. Contribution of Working Group I to the Fifth Assessment Report of the Intergovernmental Panel on Climate Change* (Cambridge: Cambridge University Press)

Jacob D J, Crawford J H, Kleb M M, Connors V S, Bendura R J, Raper J L, Sachse G W, Gille J C, Emmons L and Heald C L 2003 Transport and chemical evolution over the pacific (TRACE-P) aircraft mission: design, execution, and first results *J. Geophys. Res.* **108** 9000

Jaffe D, McKendry I, Anderson T and Price H 2003 Six 'new' episodes of trans-pacific transport of air pollutants *Atmos. Environ.* **37** 391–404

Jahaya M F, Mohamad M and Ying T Y 2013 The greenhouse gases observation and analysis at GAW stations in Malaysia *Asian GAW Greenhouse Gases Newsletter* vol 4 (Seoul, Korea: Korea Meteorological Administration) pp 35–40

Kondo Y, Ko M, Koike M, Kawakami S and Ogawa T 2002 Preface to special section on Biomass Burning and Lightning Experiment (BIBLE) *J. Geophys. Res.* **108** 8397

Kuze A, Suto H, Nakajima M and Hamazaki T 2009 Thermal and near infrared sensor for carbon observation Fourier-transform spectrometer on the Greenhouse gases observing satellite for greenhouse gases monitoring *Appl. Optics* **48** 6716–33

Lawrence M G 2004 Export of air pollution from Southern Asia and its large-scale effects *The Handbook of Environmental Chemistry* ed A Stohl (Heidelberg: Springer) pp 131–72

Liang Q, Jaegle L, Jaffe D A, Weiss-Penzias P, Heckman A and Snow J A 2004 Long-range transport of Asian pollution to the northeast pacific: seasonal variations and transport pathways of carbon monoxide *J. Geophys. Res.* **109** D23S07

Lin N H, Sayer A M, Wang S H, Loftus A M, Hsiao T C, Sheu G R, Hsu N C, Tsay S C and Chantara S 2014 Interactions between biomass-burning aerosols and clouds over Southeast Asia: current status, challenges, and perspectives *Environ. Pollut.* **195** 292–307

Lin N H *et al* 2013 An overview of regional experiments on biomass burning aerosols and related pollutants in Southeast Asia: from BASE-ASIA and the Dongsha experiment to 7-SEAS *Atmos. Environ.* **78** 1–19

Liu H Y, Jacob D J, Bey I, Yantosca R M, Duncan B N and Sachse G W 2003 Transport pathways for Asian pollution outflow over the pacific: interannual and seasonal variations *J. Geophys. Res.* **108** 8786

Liu Z, Yang H and Liu Q 2001 Regional dynamics of seasonal variability in the South China Sea *J. Phys. Oceanogr.* **31** 272–84

Matthews H D, Weaver A J, Meissner K J, Gillett N P and Eby M 2004 Natural and anthropogenic climate change: incorporating historical land cover change, vegetation dynamics and the global carbon cycle *Clim. Dynam.* **22** 461–79

Metzger E J 2003 Upper ocean sensitivity to wind forcing in the South China Sea *J. Oceanogr.* **59** 783–98

Morino I *et al* 2011 Preliminary validation of column-averaged volume mixing ratios of carbon dioxide and methane retrieved from GOSAT short-wavelength infrared spectra *Atmos. Meas. Tech.* **4** 1061–76

Moron V, Robertson A W and Boer R 2009 Spatial coherence and seasonal predictability of monsoon onset over Indonesia *J. Climate* **22** 840–50

Nahas A C 2012 Greenhouse gases monitoring activies at global GAW station Bukit Kototabang, Indonesia *Asian GAW Greenhouse Gases Newsletter* vol 3 (Seoul, Korea: Korea Meteorological Administration) pp 12–4

Nakajima T *et al* 2007 Overview of the atmospheric brown cloud east asian regional experiment 2005 and a study of the aerosol direct radiative forcing in east Asia *J. Geophys. Res.* **112** D24S91

Nisbet E G, Dlugokencky E J and Bousquet P 2014 Methane on the rise-again *Science* **343** 493–5

Ohara T, Akimoto H, Kurokawa J, Horii N, Yamaji K, Yan X and Hayasaka T 2007 An Asian emission inventory of anthropogenic emission sources for the period 1980-2020 *Atmos. Chem. Phys.* **7** 4419–44

Olivier J G J, Janssens-Maenhout G, Muntean M and Peters J A H W 2014 *Trends in global CO_2 emissions: 2014 Report* (Hague, Netherlands: PBL)

Ou-Yang C F, Lin N H, Sheu G R, Lee C T and Wang J L 2012 Seasonal and diurnal variations of ozone at a high-altitude mountain baseline station in East Asia *Atmos. Environ.* **46** 279–88

Ou-Yang C F, Hsieh H C, Wang S H, Lin N H, Lee C T, Sheu G R and Wang J L 2013 Influence of Asian continental outflow on the regional background ozone level in northern South China Sea *Atmos. Environ.* **78** 144–53

Ou-Yang C F, Lin N H, Lin C C, Wang S H, Sheu G R, Lee C T, Schnell R C, Lang P M, Kawasato T and Wang J L 2014 Characteristics of atmospheric carbon monoxide at a high-mountain background station in East Asia *Atmos. Environ.* **89** 613–22

Palm C A, Alegre J C, Arevalo L, Mutuo P K, Mosier A R and Coe R 2002 Nitrous oxide and methane fluxes in six different land use systems in the Peruvian Amazon *Global. Biogeochem. Cy.* **16** 1073

Parker R *et al* 2011 Methane observations from the Greenhouse gases observing satellite: comparison to ground-based TCCON data and model calculations *Geophys. Res. Lett.* **38** L15807

Pochanart P, Akimoto H, Kajii Y, Potemkin V M and Khodzher T V 2003 Regional background ozone and carbon monoxide variations in remote Siberia/East Asia *J. Geophys. Res.* **108** 024020

Reid J S, Xian P, Hyer E J, Flatau M K, Ramirez E M, Turk F J, Sampson C R, Zhang C, Fukada E M and Maloney E D 2012 Multi-scale meteorological conceptual analysis of observed active fire hotspot activity and smoke optical depth in the maritime continent *Atmos. Chem. Phys.* **12** 2117–47

Reid J S *et al* 2013 Observing and understanding the Southeast Asian aerosol system by remote sensing: an initial review and analysis for the Seven Southeast Asian Studies (7SEAS) program *Atmos. Res.* **122** 403–68

Reisinger A, Meinshausen M and Manning M 2011 Future changes in global warming potentials under representative concentration pathways *Environ. Res. Lett.* **6**

Rigby M *et al* 2008 Renewed growth of atmospheric methane *Geophys. Res. Lett.* **35** L22805

Stohl A 1998 Computation, accuracy and applications of trajectories—A review and bibliography *Atmos. Environ.* **32** 947–66

Thoning K W, Tans P P and Komhyr W D 1989 Atmospheric carbon dioxide at Mauna Loa Observatory: 2. Analysis of the NOAA GMCC data, 1974–1985 *J. Geophys. Res.* **94** 8549–65

Thoning K W, Conway T J, Zhang N and Kitzis D 1995 Analysis system for measurement of CO_2 mixing ratios in flask air samples *J. Atmos. Ocean. Tech.* **12** 1349–56

Tsay S C *et al* 2013 From BASE-ASIA toward 7-SEAS: a satellite-surface perspective of boreal spring biomass-burning aerosols and clouds in Southeast Asia *Atmos. Environ.* **78** 20–34

US EIA 2013 *South China Sea* (Washington, DC: US Department of Energy)

Vay S A *et al* 2003 Influence of regional-scale anthropogenic emissions on CO_2 distributions over the western North Pacific *J. Geophys. Res.* **108** 8801

Veldkamp E, Purbopuspito J, Corre M D, Brumme R and Murdiyarso D 2008 Land use change effects on trace gas fluxes in the forest margins of Central Sulawesi, Indonesia *J. Geophys. Res.* **113** G02003

Verchot L V, Davidson E A, Cattanio J H and Ackerman I L 2000 Land-use change and biogeochemical controls of methane fluxes in soils of eastern Amazonia *Ecosystems* **3** 41–56

Wai K M and Tanner P A 2014 Recent springtime regional CO variability in Southern China and the adjacent ocean: Anthropogenic and biomass burning contribution *Aerosol. Air Qual. Res.* **14** 21–32

Wang T, Ding A J, Blake D R, Zahorowski W, Poon C N and Li Y S 2003 Chemical characterization of the boundary layer outflow of air pollution to Hong Kong during February-April 2001 *J. Geophys. Res.* **108** 8787

Wang T, Wei X L, Ding A J, Poon C N, Lam K S, Li Y S, Chan L Y and Anson M 2009 Increasing surface ozone concentrations in the background atmosphere of Southern China, 1994-2007 *Atmos. Chem. Phys.* **9** 6217–27

Wild O and Akimoto H 2001 Intercontinental transport of ozone and its precursors in a three-dimensional global CTM *J. Geophys. Res.* **106** 27729–44

Wunch D *et al* 2011 A method for evaluating bias in global measurements of CO_2 total columns from space *Atmos. Chem. Phys.* **11** 12317–37

Yen M C, Peng C M, Chen T C, Chen C S, Lin N H, Tzeng R Y, Lee Y A and Lin C C 2013 Climate and weather characteristics in association with the active fires in northern Southeast Asia and spring air pollution in Taiwan during 2010 7-SEAS/Dongsha Experiment *Atmos. Environ.* **78** 35–50

Yokota T, Yoshida Y, Eguchi N, Ota Y, Tanaka T, Watanabe H and Maksyutov S 2009 Global concentrations of CO_2 and CH_4 retrieved from GOSAT: First preliminary results *Sola* **5** 160–3

Yoshida Y *et al* 2013 Improvement of the retrieval algorithm for GOSAT SWIR XCO_2 and XCH_4 and their validation using TCCON data *Atmos. Meas. Tech.* **6** 1533–47

Zhai W D, Dai M H, Cai W J, Wang Y C and Hong H S 2005 The partial pressure of carbon dioxide and air-sea fluxes in the northern South China Sea in spring, summer and autumn *Mar. Chem.* **96** 87–97

Zhang Y, Sperber K R and Boyle J S 1997 Climatology and interannual variation of the East Asian winter monsoon: results from the 1979-95 NCEP/NCAR reanalysis *Mon. Weather. Rev.* **125** 2605–19